TOUGH3-FLAC3D: A MODELING APPROACH FOR PARALLEL COMPUTING OF FLUID FLOW AND GEOMECHANICS

Antonio P. Rinaldi[1,2*], Jonny Rutqvist[2], Keurfon Luu[2], Laura Blanco-Martín[2,3], Mengsu Hu[2], Manuel L. Sentís[4]

[1] Swiss Seismological Service, Swiss Federal Institute of Technology, ETHZ, Zurich, Switzerland

e-mail: antoniopio.rinaldi@sed.ethz.ch

[2]Energy Geosciences Division, LBNL, Berkeley, CA, USA

e-mail: jrutqvist@lbl.gov, keurfonluu@lbl.gov, mengsuhu@lbl.gov

[3]Department of Geosciences, MINES ParisTech, Fontainebleau, France

e-mail: laura.blanco_martin@mines-paristech.fr

[4]Swiss Federal Nuclear Safety Inspectorate (ENSI), Brugg, Switzerland

e-mail: manuel.sentis@ensi.ch

(*) Corresponding author at: Swiss Seismological Service, ETHZ, Sonneggstrasse 5, Zurich, Switzerland

Submitted to Computational Geosciences

ABSTRACT

The recent development of the TOUGH3 code allows for a faster and more reliable fluid flow simulator. At the same time, new versions of FLAC3D are released periodically, allowing for new features and faster execution. In this paper, we present the first implementation of the coupling between TOUGH3 and FLAC3Dv6/7, maintaining parallel computing capabilities for the coupled fluid flow and geomechanical codes. We compare the newly developed version with analytical solutions and with the previous approach, and provide some performance analysis on different meshes and varying the number of running processors. Finally, we present two case studies related to fault reactivation during CO_2 sequestration and nuclear waste disposal. The use of parallel computing allows for meshes with a larger number of elements, and hence more detailed understanding of thermo-hydro-mechanical processes occurring at depth.

Keywords: THM processes; coupled simulator; parallel computing; TOUGH3; FLAC3D

1. INTRODUCTION

The current development of georesources exploitation strongly relies on numerical simulation of the processes occurring at depth. Understanding of the coupled thermo-hydro-mechanical processes is essential to assess properly the changes in system conditions as well as to study the risks associated with the underground exploitation (e.g. loss of circulation; caprock failure; induced seismicity). Model developments and their applications constitute a huge step towards understanding coupled processes. Several numerical simulators are already available in the literature for the study of coupled processes at various levels of complexity. Some models allow for all Thermo-Hydro-Mechanical-Chemical (THMC) couplings.

Examples are: TOUGHREACT-FLAC3D (Taron and Elsworth, 2009; Rutqvist et al., 2014; Rutqvist, 2017), OpenGeoSys (Kolditz et al., 2012), Dumux (Flemisch et al., 2011), COMSOL Multiphysics (COMSOL, 2020). In addition, other simulators have been applied to study partial processes coupling, THM or THC: e.g. Sierra Mechanics (Newell et al., 2017), 3DEC (Itasca, 2016), CODE-BRIGHT (Olivella et al., 1996), CSMP++ (Yapparova et al., 2017; Salimzadeh et al., 2018), PFLOTRAN (Lichtner et al., 2017).

In numerical modelling, the governing equations (conservation laws of mass, momentum and energy) are solved considering the relationship among processes (e.g. coupling of two or more processes), and completed with constitutive laws, initial conditions and boundary conditions. One factor determining the computational effort is the number of simulated THMC coupled processes. Another factor is the numerical scheme. In the literature, the term *monolithic* refers to a scheme in which the physical equations for multiple processes are solved simultaneously, which may be computationally expensive. More loose couplings exist, such as one-way (i.e. a given process influences another, but not vice versa) or two-way sequential (i.e. the different processes are considered in sequence). Such schemes are less computationally intensive and may refer to the same simulator, but often the integration of different codes is used to take advantage of specialized codes and to increase the types of simulated processes (Kulik et al., 2012; Rutqvist, 2017).

Given the complexity of the coupled processes, verification of the numerical approach is often an issue. Analytical solutions are only available for vey simplified processes (e.g. only for fully saturated medium), and observations from lab and *in situ* experiments involve significant uncertainties. Benchmarking activities involving code-to-code comparison and validation against analytical solutions and experimental data are often in play for developing numerical models (Blanco-Martín et al., 2015; Garitte et al., 2017; Rutenberg et al., 2018; Birkholzer et al., 2019). The TOUGH family of codes are commonly applied to model the

75 coupling of fluid flow and heat transport in geological media (Pruess et al., 2012; Jung et al.,
76 2017), and have been extended to consider coupling to geomechanical processes. In
77 particular, several TOUGH-based geomechanical codes have been developed to solve THM
78 problems (Rutqvist, 2017), among which TOUGH-FLAC is the most widely used, with
79 recent applications featuring inverse modeling (Blanco-Martín et al., 2016; Rinaldi et al.,
80 2017) and finite strain deformation (Blanco-Martín et al., 2017). Since its initial development
81 in the late 1990s (Rutqvist et al., 2002), TOUGH-FLAC has been applied to study
82 geomechanical aspects of CO_2 sequestration, nuclear waste disposal, enhanced geothermal
83 systems, underground gas storage and compressed air energy storage, gas production from
84 hydrate-bearing formations, induced seismicity, as well as for the implementation and the
85 study of constitutive equations (Rutqvist, 2017 and references therein).
86 The most common version of TOUGH-FLAC accounts for the two-way sequential coupling
87 of TOUGH2 (Pruess et al., 2012) for the simulation of non-isothermal, multi-phase and
88 multi-component fluid flow with upgraded versions of FLAC3D (e.g. ver.4/5, Itasca, 2011)
89 for solving the mechanical equilibrium. The equations for fluid flow and geomechanics are
90 solved sequentially, and the approach is unconditionally stable, using the fixed-stress split
91 sequential scheme: the flow sub-problem is solved first with a fixed total stress field, which is
92 then modified in the subsequent geomechanics sub-problem by using modified variables from
93 the flow step (Kim et al., 2011).
94 Despite the wide use of TOUGH-FLAC coupled simulations in the literature, applications are
95 often limited to a relatively small computational domain, with a number of elements usually
96 smaller than 50,000. In this work, we moved one step forward by coupling for the first time
97 the newly developed TOUGH3 (Jung et al., 2017) with versions 6.0 and 7.0 of FLAC3D
98 (Itasca, 2017), hence implementing a parallelized version of the well-known coupled
99 simulator. The coupled simulator integrates all the new functionalities of TOUGH3,

including the use of PETSc solvers, together with the improved solver performance in FLAC3Dv6/7 as well as the possibility of using Python scripting compared to the FISH programming embedded in previous versions of FLAC3D. After verifying the correctness of the approach comparing the simulation results with an analytical solution and with the previous version, we evaluate the performance of the newly developed approach. Finally, we present results of two case studies, aimed at understanding the potential for fault reactivation during CO_2 sequestration and the evolution of stress and strain during nuclear waste disposal in a deep geological repository.

2. COUPLING APPROACH

The main modifications of the approach compared to the previous versions are:

1- Use of TOUGH3 with parallel computing and use of FLAC3Dv6/7, both allowing for faster calculation.

2- Use of binary instead of ASCII exchange files. This is particularly important when dealing with computational domains containing a large number of elements.

3- Use of a flag system to avoid saving and restoring the FLAC3D model state to a binary file at each time step. In the new approach, the FLAC3D model state is only loaded at the beginning of the simulation, then paused during TOUGH3 execution, thereby avoiding overhead caused by restoring/saving the mechanical state at each time step.

4- Use of Python routines to read/write coupling files in FLAC3D. Through the use of NumPy (Harris et al., 2020), this can produce up to 34× faster execution (10× in average) in variable allocation compared to the previously used FISH scripting (Itasca, 2017).

One of the limitations of FLAC3D is that it runs only on Windows-based machines. Then, to make use of the MPI parallelization provided in TOUGH3, we compiled the code in the

Cygwin environment or Windows Subsystem for Linux (Windows 10), which also allows calls to Windows executables (i.e. FLAC3D batch). All the simulations presented here were carried out on a workstation with two 6-core CPUs Intel Xeon E5-2643 (24 threads) at 3.40 GHz and equipped with 64 GB RAM.

This hardware configuration allows using up to 12 processors. Each of the two codes, evaluated separately, provides a speed increase up to 6× for a quite large computational domain (800,000 elements) on this machine when employing the maximum number of cores (supplementary material, Fig. S1).

The general coupling approach between any TOUGH-code and FLAC3D is based on file exchange to share variables and/or properties. In MPI codes, and in particular for TOUGH3, a processor is designed as "IOProcessor" and takes care of all the input/output functionalities of the code. Figure 1 describes the coupling approach for TOUGH3 and FLAC3D.

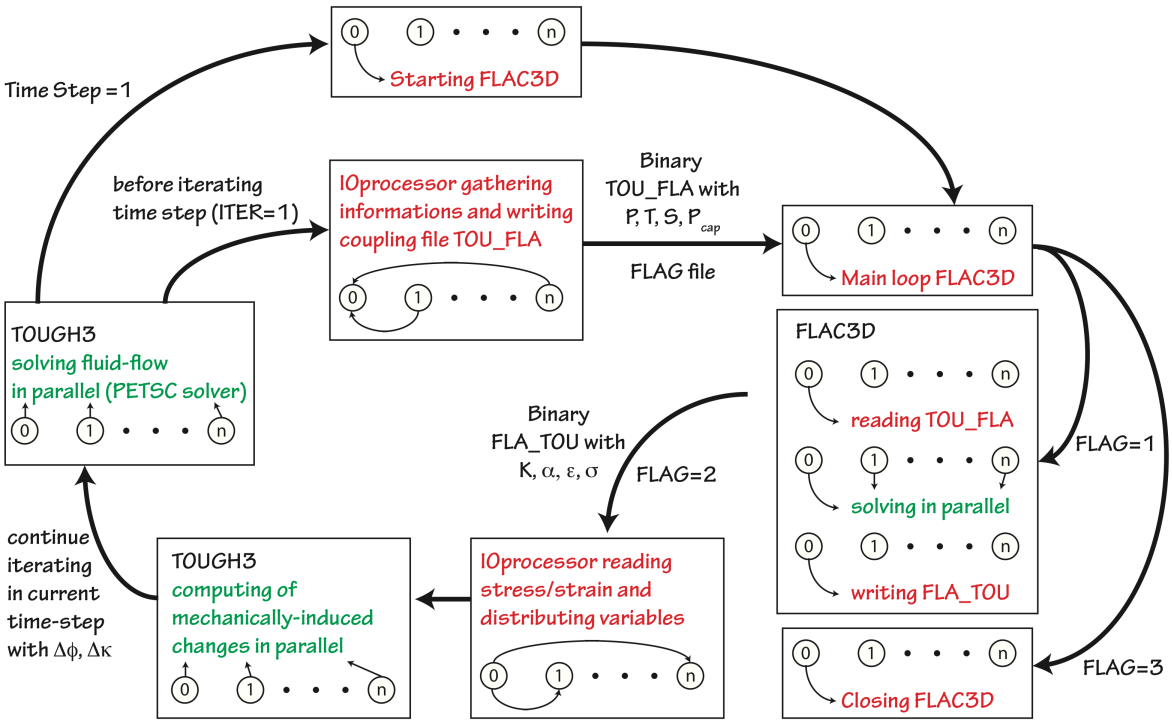

Figure 1. Coupling approach between TOUGH3 and FLAC3D for each time step. Green parts are executed in parallel, while red parts are executed in serial. P, T, S, P_{cap} are pore pressure, temperature, saturation, and capillary pressure, respectively. K, α, ε, σ, refer to bulk modulus, Biot's coefficient, strain, and stress, while $\Delta\phi$ and $\Delta\kappa$ stand for porosity and permeability changes.

As in previous versions of TOUGH-FLAC, TOUGH3 is the main code, which runs the simulation through time and modifies the time step according to the stability of the fluid flow sub-problem. At each time step, FLAC3D computes the mechanical equilibrium to a predefined convergence threshold. As a rule of thumb, the approach is quite stable for poro-elastic problems, but it may require an appropriate choice of time stepping when including time-dependent deformation (e.g. creep).

For each time step, before starting the iterations for solving the fluid flow sub-problem, TOUGH3 invokes a subroutine to gather the arrays from all the MPI processes. Such arrays (pressure, temperature, saturation and capillary pressure) are written to file TOU_FLA by the IOProcessor, together with a flag (1). The IOProcessor performs this entire stage in serial, while all the other *n* MPI processes are idle. During this process, FLAC3D is idle waiting for the flag to change. Then, FLAC3D (i) reads the TOU_FLA file (in serial), (ii) solves for mechanical equilibrium (in parallel), and (iii) writes the FLA_TOU file to transfer data to TOUGH3 (in serial), and modifies the flag (2). At this stage, the subroutine invoked previously by TOUGH3 is waiting for FLAC3D to finish execution, then the IOProcessor serially reads the flag and the FLA_TOU file and distributes the variables/properties (bulk modulus, Biot's coefficient, strain, and stress) to all *n* MPI processes.

Finally, the parallel computing can restart with the calculation of mechanically-induced changes of flow properties and with continuation of the flow iterations to finish the current time step. When TOUGH3 is at the last time step, it will issue a flag (3) that FLAC3D will interpret and save the final state in a binary file. The mechanical state as well as the flow variables can also be saved at predefined times during execution. The use of Python routines within FLAC3D allows for easier handling of arrays (e.g. mapping of a given variable or extra post-processing computation), and also for handling and personalizing the entire output functions, making redundant the use of classical TOUGH3 output functions.

3. VERIFICATION AND PERFORMANCE

3.1 Analytical solution

An analytical solution can be derived for a Terzaghi-like problem (Lux et al., 2015). The problem here is part of the BenVaSim initiative to verify and benchmark several numerical codes (Rutenberg et al., 2018). While being a simplified numerical exercise, the model setup physically resembles a dam construction in a flooded drift with a pore pressure gradient allowing water flowing through the host rock. As the current approach is based on previous versions, more verifications can be found elsewhere (Blanco-Martín et al., 2017).

The model is one dimensional, fully saturated 10 m–long domain with displacement completely fixed in *y*- and *z*- directions and at x = 10 m. The initial pressure and total stress in the model are set to 0.1013 MPa. Pore pressure is 1 MPa at left boundary (x = 0 m), and 0.1013 MPa at the right boundary (x = 10 m). A total stress of 1 MPa is applied at time $t=0^+$ at x = 0 m. The base case scenario accounts for a porous and low permeable material (porosity ϕ = 0.15; permeability $\kappa = 10^{-20}$ m^2) with stiff and deformable matrix (Young's modulus E = 8 GPa; Biot's coefficient α = 1, and Poisson's ratio v = 0 to allow for 1D problem). Variations to the base case account for compressible grains (Biot's coefficient α = 0.75) and for very soft material (Young's modulus E = 150 MPa).

Figure 2 shows the profiles of the pore pressure at different times comparing the numerical (solid line) and the analytical (shaded area) solutions. Results show that for different times, the developed approach is able to match the analytical solution, with only minor differences mostly related to space discretization (50 elements for the 10 m long domain). The initial pressurization of the system (undrained response at 0.003 *y*) is somewhat larger than the analytical solution due to coarse time discretization, while the steady state is well matched (at 30 y for the base case scenario). A more compressible grain will result in less undrained

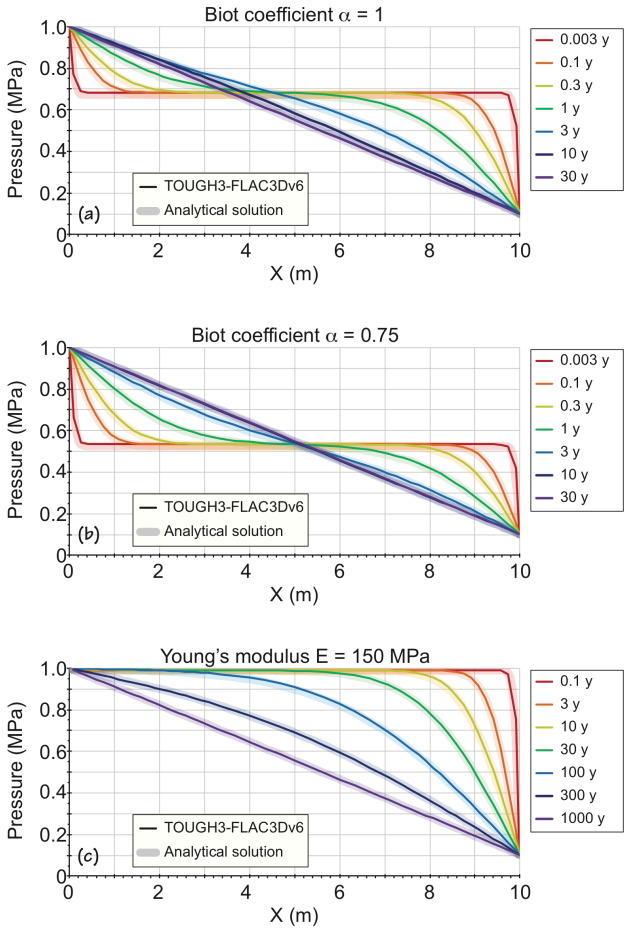

Figure 2. Verification of the coupling approach with an analytical solution in a low permeable environment. (a) Base case scenario; (b) Compressible grains (Biot coefficient $\alpha = 0.75$); (c) Soft matrix (Young's modulus E= 150 MPa).

pressurization (Fig. 2b), while the soft matrix will result in much larger deformation, allowing for larger porosity decrease in the matrix, and larger pressure increase during the undrained response (Fig. 2c). As it can be seen, the numerical approach is in good agreement with the analytical solution also for more critical scenarios.

3.2 Comparison with previous simulator

In order to verify the validity of TOUGH3-FLAC3Dv6/7, we compared results with the previous TOUGH2-FLAC3Dv5 (Blanco-Martín et al., 2017). We checked the results for variables such as injection pressure and temperature as well as the uplift of the top boundary.

We account for a 3D computational domain (10 km × 10 km × 4 km) with homogeneous properties (permeability $\kappa = 5 \cdot 10^{-15}$ m^2, porosity $\phi = 0.1$, density $\rho = 2550$ kg/m^3). The model ranges from a depth of -2 km to -6 km, and top and bottom boundaries, as well as the boundaries at $x = y = 10$ km, are open to fluid flow. The boundaries at $x = y = 0$ km are closed and allow for symmetry. Mechanically, we assume a poro-elastic material (Young's modulus $E = 10$ GPa, Poisson's ratio $\nu = 0.25$, Biot's coefficient $\alpha = 1$), with the top and side boundaries ($x = y = 10$ km) at fixed stress conditions, with rollers for all the other boundaries. We assume initial hydrostatic gradient for pore pressure, geothermal gradient for temperature (30 ˚C/km), and lithostatic gradient for stresses. We simulate 60 days of cold-water injection (T = 10 ˚C) in a saturated medium with variable rate (30 days at 30 kg/s, 20 days at 60 kg/s, and 10 days at 90 kg/s), followed by 40 days of shut-in period for a total simulation time of 100 days. The injection region is at a depth of 4 km and extends over a region 50 m × 50 m × 50 m. For both simulations, we use a mesh with ~46,500 elements. Porosity changes depend on the bulk modulus and on the total volumetric strain, when larger than 10^{-4}. The FLAC3D mechanical ratio between the maximum unbalanced force magnitude and the average applied force magnitude is set to 10^{-7}. The TOUGH3 convergence criterion is set to 10^{-5}.

As shown in Figure 3, the two approaches are in extremely good agreement, with differences in pressure in the order of some Pa, minor differences in temperature, and differences in uplift in the order of some microns.

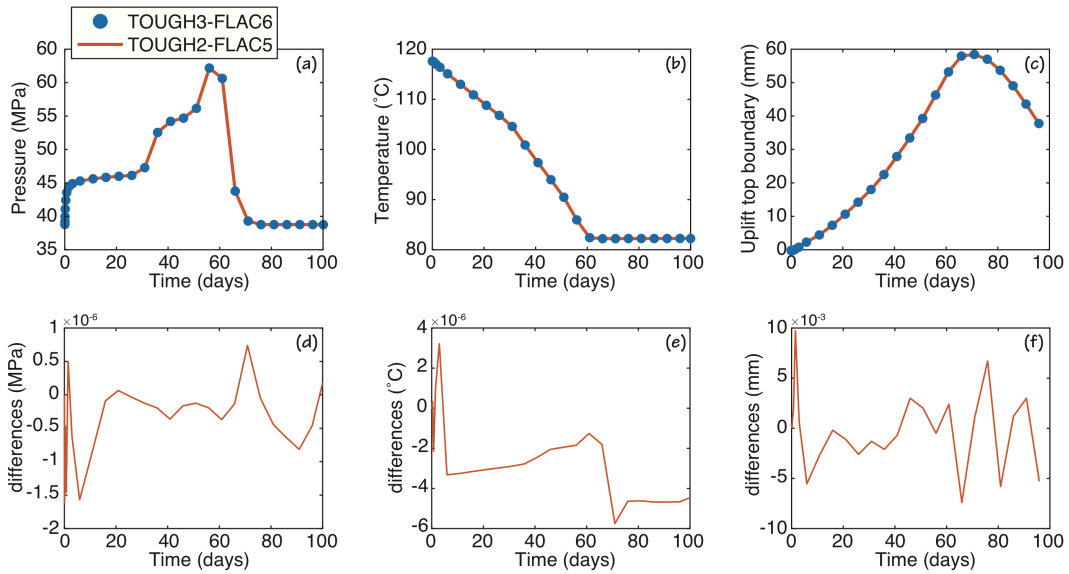

Figure 3. Comparison between TOUGH2-FLAC3Dv5 (red line) and TOUGH3-FLAC3Dv6 (blue dots) for pressure near the injection point (a), temperature near the injection point (b), and uplift of the top boundary (c) for a mesh with 46,464 elements. (d-f): differences between the two approaches.

3.3. Performance Tests

Figure 4a-b show the performance of TOUGH3-FLAC3Dv6 compared to the previous version and to serial execution as a function of number of threads and for various sizes of the computational domain. We varied the number of threads in FLAC3D and the number of cores in TOUGH3 accordingly (each core allows for two threads). For each computational domain, we have created similar initial conditions (via steady state simulation), to avoid biases on the final simulation, which is the same as what was described in Section 3.2. Some differences may arise for small meshes in the final displacement, which depends on the exact position of the monitoring point, which is set the nearest to the position x=300 m, y=300 m, and z=-2000 m (supplementary material, Fig. S2). For a single core and thread, the code is 1.5x faster compared to the previous version only owing to better I/O handling and use of Python in FLAC3D. Due to parallelization overhead (communication and domain decomposition), the speed up clearly depends on the size of the mesh, with an increase of up to 2× faster for a coarse mesh with 4,000 elements and up to 4× faster for a relatively fine

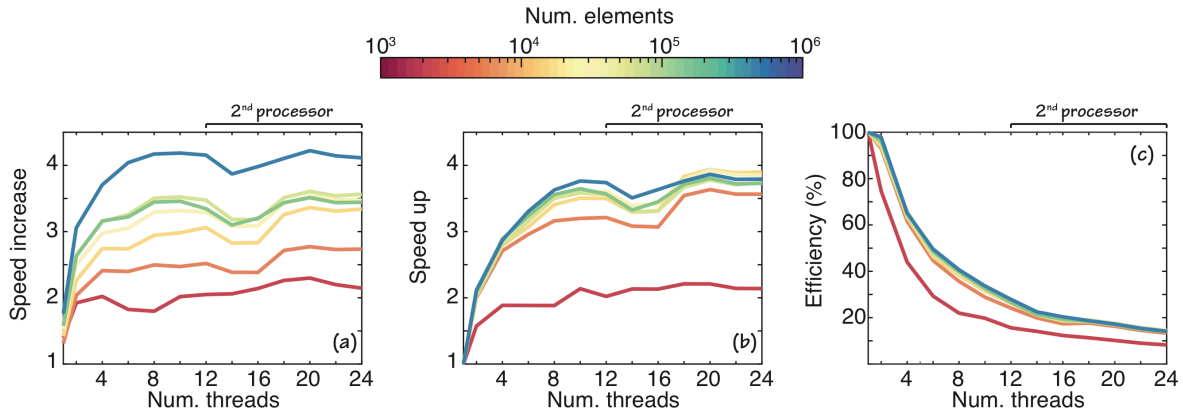

Figure 4. (a) Speed increase for TOUGH3-FLAC3Dv6 compared to TOUGH2-FLAC3Dv5 as a function of the number of threads for different mesh sizes (colormap). (b) Speed up of the current approach (execution time for a single thread compared to multi-thread) as a function of number of threads for different mesh sizes (colormap) (c) Efficiency of TOUGH3-FLAC3Dv6 for different mesh sizes (colormap)

mesh with 800,000 elements. Interestingly, for all the cases the performances do not improve after reaching 12 threads (6 cores). This could be linked to the configuration of the workstation used for testing, that accounts for two 6-core processors. In fact, FLAC3D's developers suggest the use of single processor workstation[1]. Therefore, the scaling for multiple cores is not effective past 12 threads, and the efficiency (speed up/number of cores) of the coupled approach strongly drops below 50% (Figure 4c). Overall, the speed up is not dramatically smaller when compared to what we obtain on the same workstation for using TOUGH3 or FLAC3D independently from each other: a speed increase of 6× (supplementary material, Fig. S1).

[1] https://www.itascainternational.com/software/faqs/does-itasca-software-support-multiple-processors

4. CASE STUDIES

4.1 Fault reactivation during CO_2 sequestration

The model presented here closely follows previous works addressing the same topic (Rutqvist et al., 2016). A three dimensional model was already proposed by Rinaldi et al. (2015), who addressed the effect of the well orientation on induced seismicity and CO_2 leakage through the fault. Here, thanks to the faster solver, we introduce a further complication in the model, which is the presence of a multiple fault system (Fig. 5). A similar model was also employed for studying the natural seismicity occurring at Matsushiro, Japan (Cappa et al., 2009), but here the much larger number of elements allows for better details. We simulate a 3D computational domain 10 km × 10 km × 3 km with about 1 million elements. The two fault zones strike N90° and N180° while dipping 90° and 80°, respectively, and intersect at the center of the computational domain, assuming the north is oriented in the *y*-direction. (Fig. 5). Injection occurs in a 100 m thick reservoir, bounded by

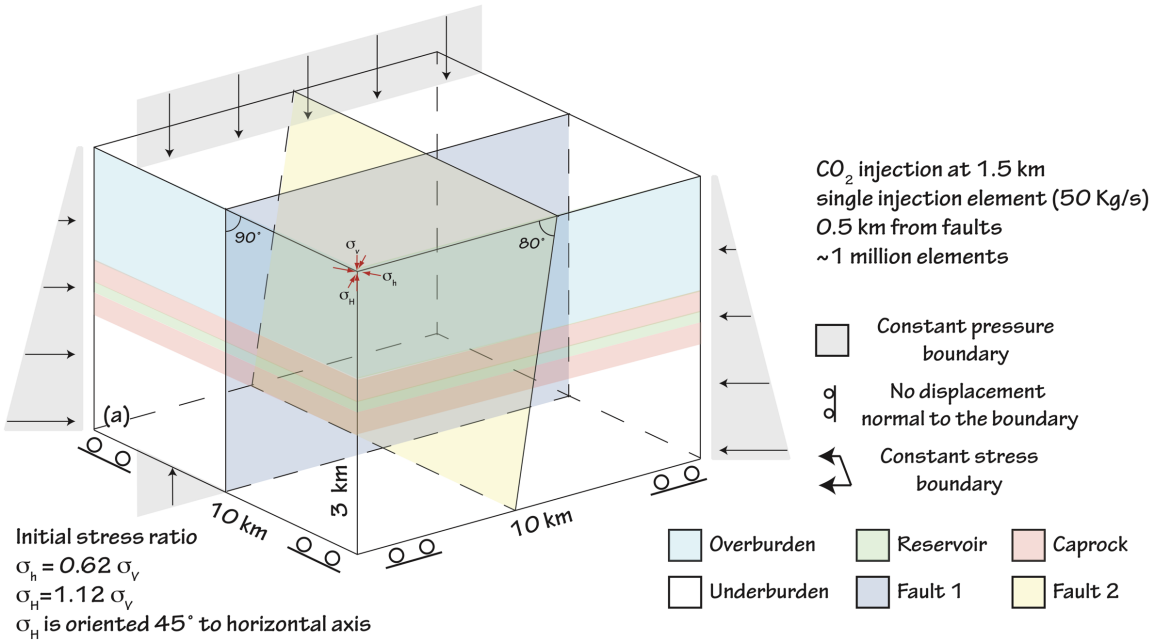

Figure 5. Computational domain for the study of fault reactivation during CO_2 injection.

two 150 m thick caprock formations, at a distance of 500 m from each fault (at a single point x = 4500 m, y = 4500 m, z = -1500 m), and with a constant rate of 50 kg/s (1.6 Mt/y) for a total of 3 years. Initial conditions account for hydrostatic pressure and geothermal gradient, and the simulation is considered isothermal (i.e., temperature is only needed to calculate the fluid viscosity and density). Initial stress follows a strike-slip regime, with both maximum and minimum principal stresses horizontal. The maximum horizontal stress (σ_H) is oriented N45° with a stress ratio σ_H/σ_V = 1.12, while the minimum horizontal stress (σ_h) has a ratio of σ_h/σ_V = 0.62, with the vertical one (σ_V) being the lithostatic stress. Boundaries are all open to fluid flow with constant lithostatic stress and hydrostatic pore pressure, except for the bottom where the displacement normal to the boundary is null. The system is initially fully saturated with brine, with retention curves for capillary pressure and relative permeability following van Genuchten (1980).

Table 1. Hydraulic and mechanical properties for the different domains in the CO_2 injection case study

	Reservoir	**Caprock**	**Overburden**	**Underburden**	**Damage zone**	**Fault core 1**	**Fault core 2**
Permeability (m^2)	10^{-13}	10^{-19}	10^{-14}	10^{-18}	10^{-15}	10^{-17}	10^{-17}
Porosity	0.1	0.1	0.1	0.1	0.1	0.1	0.1
Rock density (kg/m^3)	2260	2260	2260	2260	2260	2260	2260
Residual CO_2 saturation (-)	0.05	0.05	0.05	0.05	0.05	0.05	0.05
Residual liquid saturation (-)	0.3	0.3	0.3	0.3	0.3	0.3	0.3
van Genuchten (1980), p_0 (kPa)	19.9	621	19.9	621	19.9	19.9	19.9
van Genuchten (1980), m (-)	0.457	0.457	0.457	0.457	0.457	0.457	0.457
Young's modulus (GPa)	10	10	10	10	10	5	5
Poisson's ratio	0.25	0.25	0.25	0.25	0.25	0.25	0.25
Peak/residual friction angle (°)	-	-	-	-	-	31/29	31/29
Dilation angle (°)	-	-	-	-	-	10	10

287 For the sake of simplicity, we do not include permeability changes at this stage, as we focus
288 on the reactivation of the faults. Permeability changes are instead more relevant when
289 studying CO_2 leakage (Rinaldi et al., 2014). We account for the full hydro-mechanical
290 coupling by modeling porosity changes as function of the volumetric strain and pore
291 pressure.
292 We assume for all rock formations elastic rheology, except the core of both faults, which
293 follows a strain-softening ubiquitous-joint model with frictional law depending on the
294 accumulated plastic strain (Cappa and Rutqvist, 2011). Both elastic and hydraulic properties
295 for the different domains are listed in Table 1. The simulation execution time with the given
296 setup is comparable to a similar case in 2D and single fault for the previous version of the
297 simulator (some hours).
298 Pressure evolution and CO_2 plume are shown in Figure 6. Results show that the
299 pressurization of the reservoir is quite fast with changes up to 4 MPa near the injection point.
300 Both faults start pressurizing right after injection starts, and less than 5 MPa are needed to
301 reactivate both faults, with reactivation time depending on the fault strength (or actually on
302 the fault orientation with respect to the state of stress). The CO_2 plume is still confined close
303 to the injection, extending up to 200 m when both faults are reactivated.
304 Figure 7 shows how the rupture starts occurring on Fault 1 (the vertical blue fault, Fig. 5),
305 and it is followed several days after by reactivation on Fault 2 (the dipping yellow fault, Fig.
306 5). This is consistent with the state of stress, according to which Fault 1 is favorably oriented
307 for shear activation. Given the frictional law in the ubiquitous joint model, the friction angle
308 drops in the ruptured area (i.e. the one where plastic strain accumulates) from the peak value
309 (31°) to the residual (29°). Reactivation on Fault 1 occurs after only 30 days of injection with
310 maximum slip of 0.6 cm (Fig. 7a-b), and it is followed by the reactivation on Fault 2 after 70
311 days of injection with a maximum slip of 0.2 cm, which involves only a small minor patch on

312

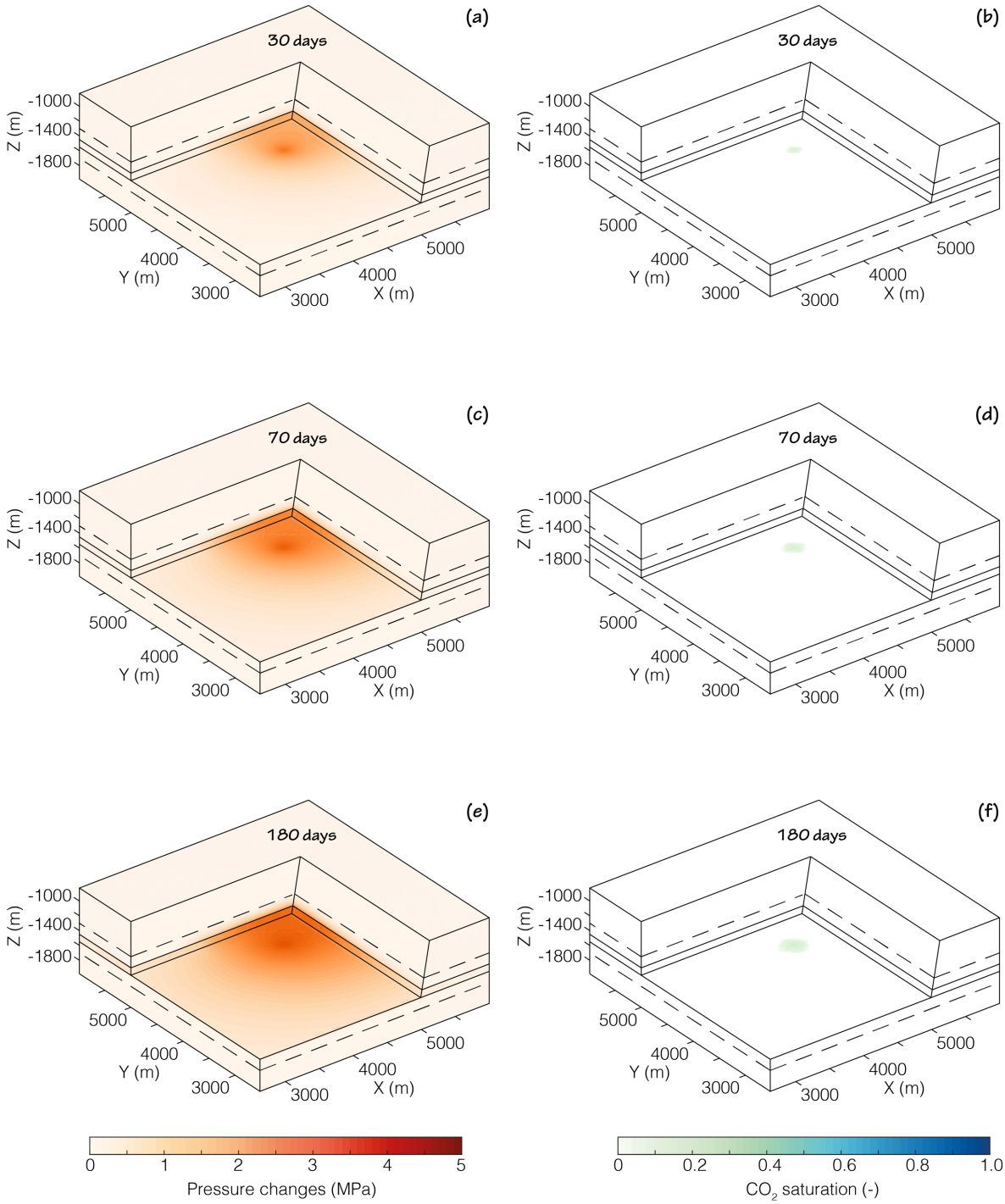

313

314 *Figure 6.* Distribution of pressure changes (a,c,e) and CO_2 saturation (b,d,f) after 30, 70, and 180 days of
315 injection operations.

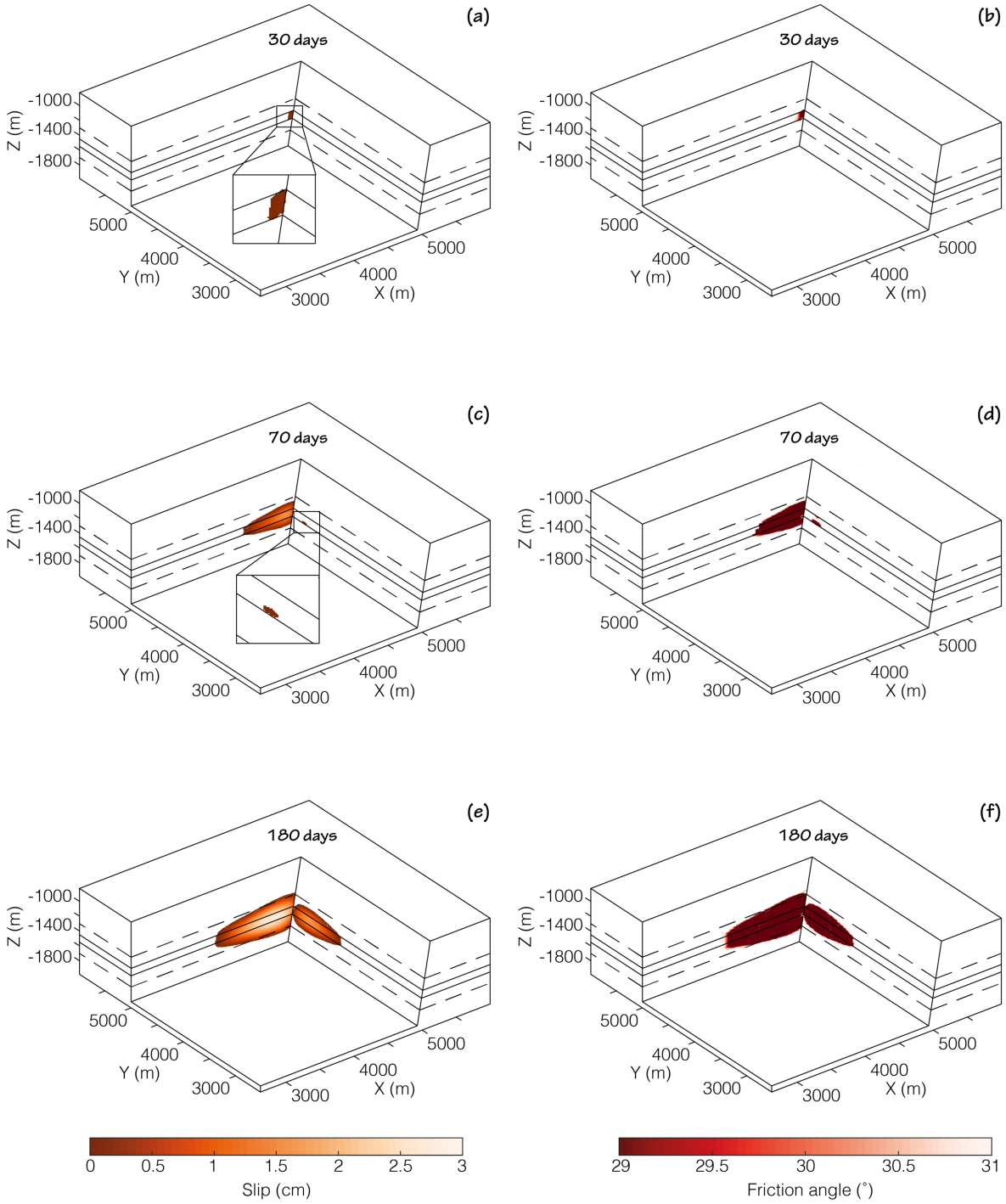

316

317 *Figure 7.* Distribution of plastic slip (a,b,c) and friction angle (d,e,f) at 30, 70, and 180 days of injection.

318 the fault plane (Fig. 7c-d). Worth to note that while the injection continues, the rupture

319 continues extending on the two faults, reaching a maximum extent after 180 days of

320 injection, which is much shorter than the total injection time of 3 years. The rupture area is

larger on Fault 1 given the more optimal orientation for shear rupture with respect to the stress field.

4.2 Potential for fault reactivation during geological nuclear waste disposal

The model presented in this section aims at understanding the stress and strain changes occurring at depth in a nuclear waste geological repository. We simulate the heat generated by several, parallel nuclear waste emplacement tunnels located in argillaceous clay host rock, i.e. following the Swiss concept for geological nuclear waste disposal (NAGRA, 2016). The use of a refined mesh allows for more details. Figure 8a shows the three-dimensional computational domain, with dimensions 10 km × 10 km × 5.5 km and starting at the ground surface. We simulate conditions during 2000 years after nuclear waste disposal in a repository located in a clay layer with anisotropic permeability at a depth of 700 m, and embedded within two seal formations as well as under- and overburden. Thanks to symmetry, we simulate only a quarter of the domain, and simulate 13 half-length tunnels. Each tunnel has a length of 450 m and the tunnels are 50 m apart. Each element of the tunnel is a heat source variable in time (Fig. 8b), and is connected to two elements of the main computational domain (Fig. 8a,). The boundaries at $x = 0$ m and $y = 0$ m are closed to fluid flow and have null displacement normal to the boundary to simulate symmetry. The other boundaries are open to fluid flow and have constant lithostatic stress and hydrostatic pore pressure, with the exception of the bottom boundary where the normal displacement is blocked, and the pore pressure is set to ~54 MPa. Initial conditions follow hydrostatic and geothermal (30 C°/km) gradients, while we impose normal stress conditions with the lithostatic vertical

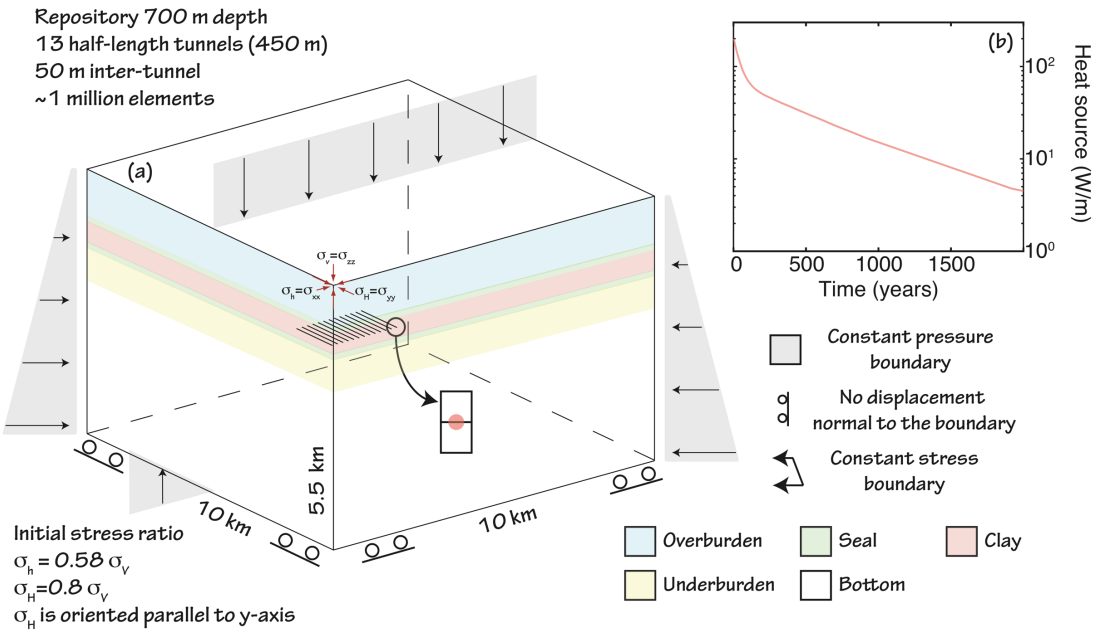

Figure 8. Computational domain for the study of potential fault reactivation during geological nuclear waste disposal.

stress (σ_V) being the maximum principal stress and with $\sigma_{xx} = \sigma_h$ as minimum principal stress. We impose stress ratios $\sigma_h / \sigma_V = 0.58$ and $\sigma_H / \sigma_V = 0.8$. We simulate full thermo-hydro-mechanical coupling by assuming that the porosity depends on strain, pressure, and temperature. We neglect at the current stage any permeability variation as a function of the stress field. For simplicity, all the layers follow an elastic rheology, and we varied only the hydraulic properties (Table 2). We use here single phase conditions, assuming that the tunnels are already fully saturated at hydrostatic pressure conditions after emplacement, i.e. ignoring some of the short-term re-saturation process that may take tens of years (Rutqvist et al., 2014) as well as potential gas generation (Fall et al., 2014; Shaw, 2015). The full 2000 years are simulated in a bit more than 2 hours.

Figure 9 shows the temperature and pore pressure distribution at different stages of evolution. Thermal effects are slower and only few °C changes are observed 10 years after emplacement in the near repository region (Fig. 9a), but the temperature changes are large enough to enable so-called thermal pressurization, a phenomenon known to occur when heating pore fluids in

Table 2. Hydraulic and mechanical properties for the different domains in the deep geological repository case study. Note that for the clay we assume anisotropic permeability.

	Soil	**Overburden**	**Seal**	**Clay**	**Underburden**	**Bottom**
Permeability (k_h/k_v) (m^2)	10^{-14}	10^{-15}	10^{-17}	$3{\cdot}10^{-19}/6{\cdot}10^{-20}$	10^{-17}	10^{-18}
Porosity	0.1	0.1	0.05	0.074	0.01	0.01
Rock density (kg/m^3)	2430	2430	2430	2430	2430	2430
Thermal conductivity (W/m °C)	3.2	3.2	3.2	3.2	3.2	3.2
Specific Heat (J/kg °C)	920	920	920	920	920	920
Young's modulus (GPa)	8	8	8	8	8	8
Poisson's ratio	0.27	0.27	0.27	0.27	0.27	0.27
Linear thermal expansion coefficient ($°C^{-1}$)	$2{\cdot}10^{-5}$	$2{\cdot}10^{-5}$	$2{\cdot}10^{-5}$	$2{\cdot}10^{-5}$	$2{\cdot}10^{-5}$	$2{\cdot}10^{-5}$

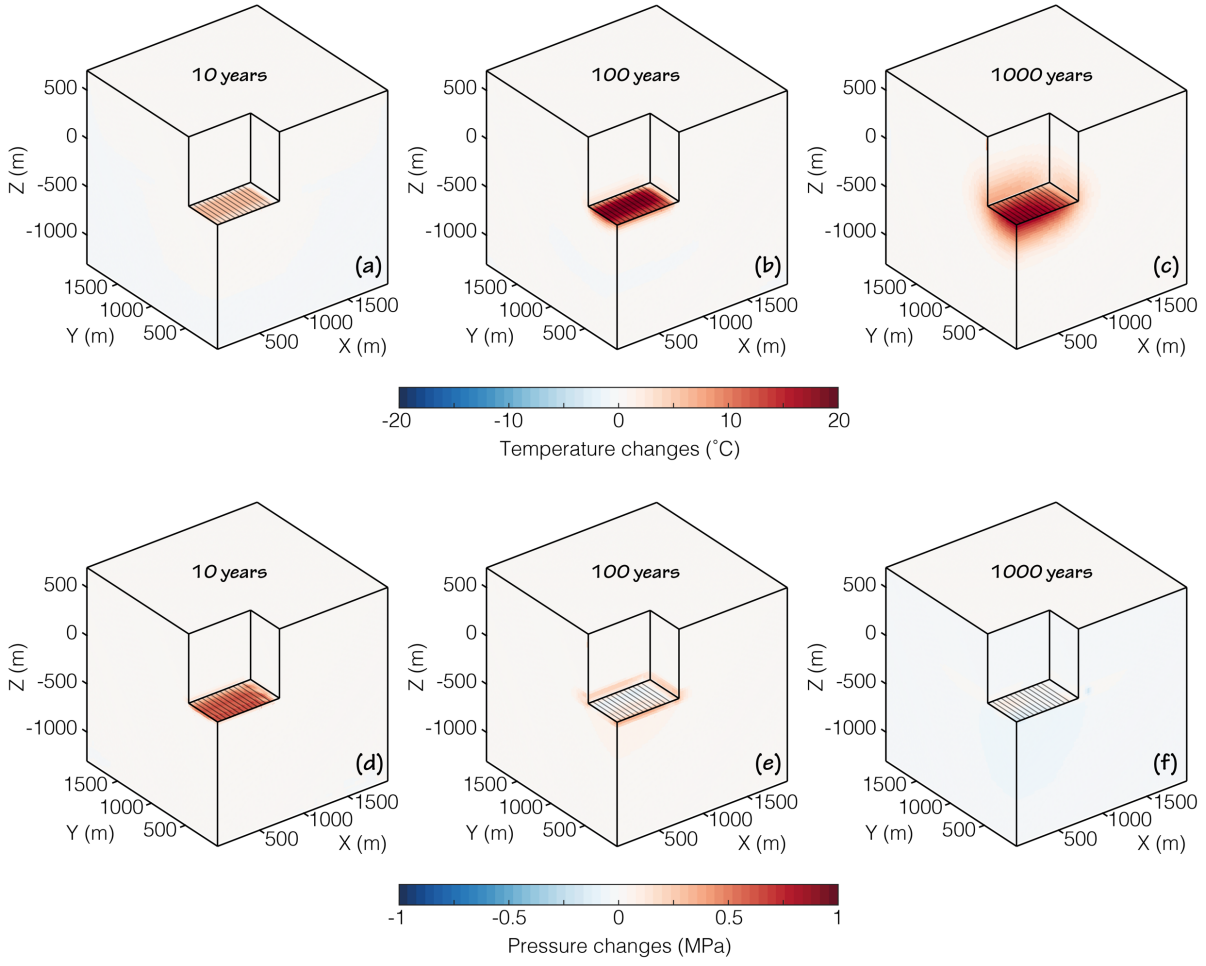

Figure 9. Distribution of changes in temperature (a,b,c) and pressure (d,e,f) in a deep geological repository for the storage of nuclear waste 10, 100, and 1000 years after emplacement.

low permeability rocks, such as shale (Gens et al., 2007; Ghabezloo and Sulem, 2009; Zhang et al., 2017). In this case, the thermal pressurization causes a relatively small pore pressure increase of about 1 MPa (Fig. 9d). The domain remains fully saturated.

At later stages, temperature changes start distributing in the domain up to several hundreds of meters outside the repository after 1000 years (Fig. 9c). At the same time, the pressure changes are diffused in the low permeable clay formation, and only minor changes are observed after 1000 years (Fig. 9f).

The temperature changes due to the heat generated by the nuclear waste can be responsible of quite large deformation at the ground surface, up to several cm uplift after 1000 years (Fig. 10a, b, and c). We also evaluated the potential for fault reactivation. Starting from the changes in the full stress tensor, we evaluate the Coulomb Stress change as $\Delta CFS = \Delta\tau + \mu(\Delta\sigma_n + \Delta p)$, where $\Delta\tau$ is the change in shear stress, $\Delta\sigma_n$ is the change in normal stress and Δp is the change in pore pressure, with the convention of stresses negative for compression. Shear and normal stresses are calculated for faults striking parallel to the tunnels and with 80° dip angle toward the repository (i.e. strike N180°). Figures 10d-f show how the repository itself is undergoing stress shadow (negative Coulomb stress changes), meaning that failure is hindered. At early times, the thermal pressurization is causing only more compression and stabilizing faults in the near repository region (Fig. 10d). Failure of the considered fault orientation is, however, favored at greater depth, where more seismogenic faults could be present. This is linked to the shear transfer caused by temperature changes, and it is then particularly relevant when the thermal effect starts distributing outside the clay formation (e.g. at 100 or 1000 years – Fig. 10e-f). These results are valid for steeply dipping faults and are well in agreement with a recent 2D study on fault reactivation during disposal of nuclear waste at depth (Urpi et al., 2019).

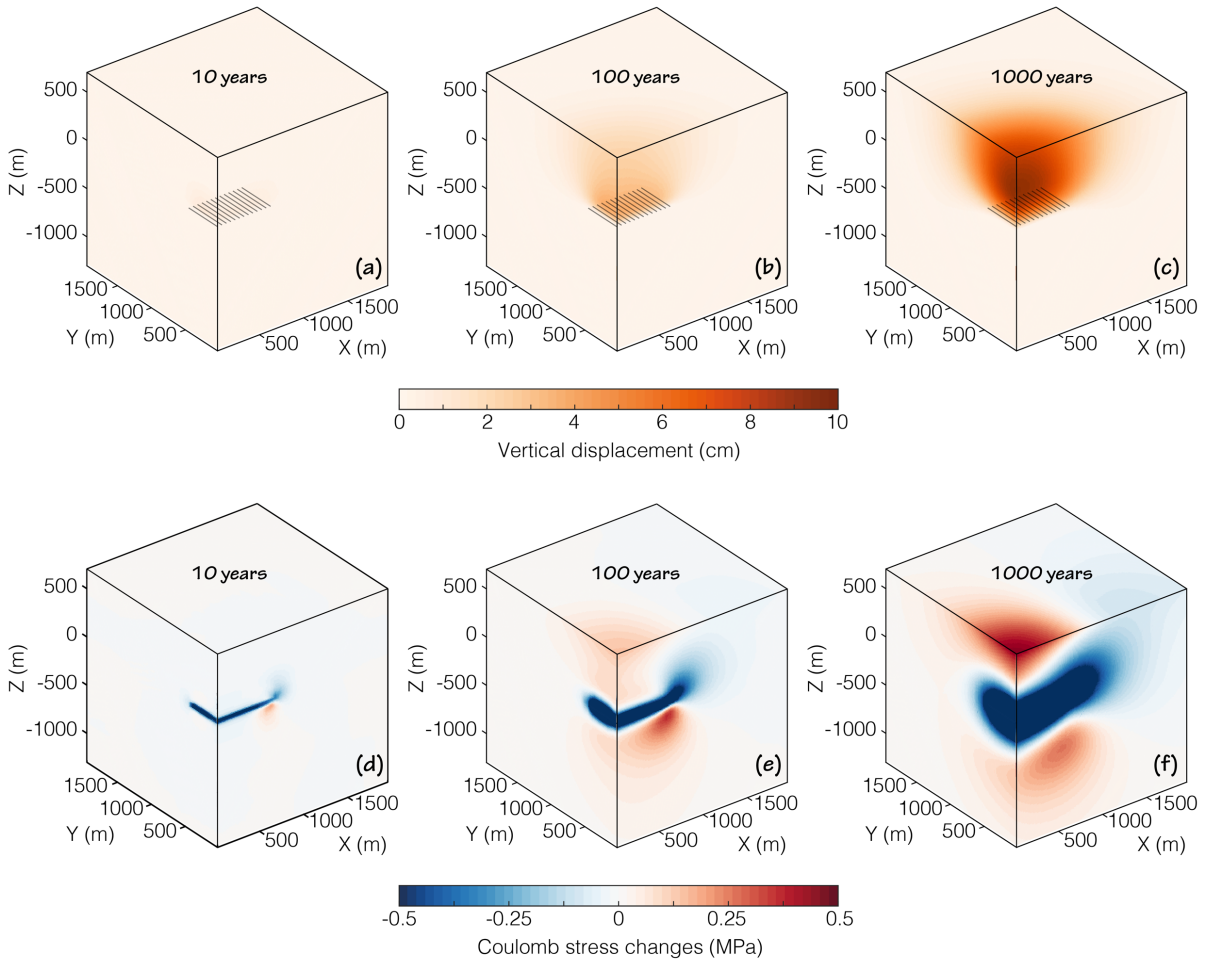

Figure 10. Distribution of vertical displacement (a,b,c) and Coulomb stress changes (d,e,f) in a deep geological repository for the storage of nuclear waste 10, 100, and 1000 years after emplacement. Coulomb stress is calculated for faults dipping 80° and striking N180°, assuming the north is oriented in the *y*-direction.

5. CONCLUSION AND FUTURE OUTLOOK

We coupled for the first time the recently released TOUGH3 with FLAC3Dv6/7. The results are well in agreement with analytical solutions and with the previous version of the simulator (TOUGH2-FLAC3Dv5). The coupled code can now use all the new functionalities of TOUGH3, including, among others, the flexibility of a Fortran 90 code and the use of PETSc. Together with the claimed improved solver performance, FLAC3Dv6/7 includes an internal link with Python scripting, which provides an average 10× faster I/O and variables assignment performance compared to the FISH programming embedded in FLAC3Dv5.

405 The removal of some bottlenecks, thanks to the use of binary files rather than ASCII, and the
406 removal of save/restore operations for FLAC3D, largely helped in improving the
407 performances of the coupled approach. The current coupled code allows up to 4-fold increase
408 in execution speed for a two 6-core processors workstation compared to the previous version
409 for a mesh with about 800,000 elements.
410 The possibility to run problems with very large number of elements in the computational
411 mesh will enable a more detailed description of the thermo-hydro-mechanical processes
412 occurring at depth. We have provided in this work two examples: one relates to fault
413 reactivation during CO_2 sequestration, and the second one relates to nuclear waste disposal.
414 For the first test case, we were able to simulate reactivation of intersecting faults during
415 injection operations. The example highlights the time of induced fault reactivation for each
416 fault. In the second test case, we demonstrate the use of the approach to simulate multiple
417 emplacement tunnels at high details. Albeit simplified, the example shows the evolution of
418 stress and strain in a deep geological nuclear waste repository, including the potential for
419 fault reactivation.
420 The current coupled code, however, does not provide yet the improved performances that
421 could be desired for High-Performance Computing in clusters. Certainly, a drawback with the
422 use of TOUGH-FLAC is the limitation to run exclusively on Windows-based machines.
423 However, Itasca plans on releasing a MPI version of their code in the future (Rutqvist, 2017),
424 and the current version of TOUGH3-FLAC3D constitutes a strong base for future coupling.
425

426 **ACKNOWLEDGMENTS**

427 The research was funded by a research agreement between ENSI and SED and by a Swiss
428 National Science Foundation (SNSF) Ambizione Energy research grant (PZENP2_160555).
429 Funding for LBNL was provided by the Spent Fuel and Waste Disposition Campaign, Office
430 of Nuclear Energy of the U.S. DOE, under Contract Number DE-AC02-05CH11231. The

authors are grateful to Michael Ruthenberg and the BenVaSim community for useful discussions.

REFERENCES

Birkholzer, J.T., Tsang, C.-F., Bond, A.E., Hudson, J.A., Jing, L., Stephansson, O., 2019. 25 years of DECOVALEX - Scientific advances and lessons learned from an international research collaboration in coupled subsurface processes. *Int. J. Rock Mech. Min. Sci.* 122, 103995. doi:10.1016/j.ijrmms.2019.03.015

Blanco-Martín, L., Rutqvist, J., Birkholzer, J.T., 2017. Extension of TOUGH-FLAC to the finite strain framework. *Comput. Geosci.* 108, 64–71. doi:10.1016/j.cageo.2016.10.015

Blanco-Martín, L., Rutqvist, J., Doughty, C., Zhang, Y., Finsterle, S., Oldenburg, C.M., 2016. Coupled geomechanics and flow modeling of thermally induced compaction in heavy oil diatomite reservoirs under cyclic steaming. *J. Pet. Sci. Eng.* 147, 474–484. doi:10.1016/j.petrol.2016.09.002

Blanco-Martín, L., Wolters, R., Rutqvist, J., Lux, K.-H., Birkholzer, J.T., 2015. Comparison of two simulators to investigate thermal–hydraulic–mechanical processes related to nuclear waste isolation in saliferous formations. *Comput. Geotech.* 66, 219–229. doi:10.1016/j.compgeo.2015.01.021

Cappa, F., Rutqvist, J., 2011. Impact of CO2 geological sequestration on the nucleation of earthquakes. *Geophys. Res. Lett.* 38, L17313. doi:10.1029/2011GL048487

Cappa, F., Rutqvist, J., Yamamoto, K., 2009. Modeling crustal deformation and rupture processes related to upwelling of deep CO2-rich fluids during the 1965–1967 Matsushiro earthquake swarm in Japan. *J. Geophys. Res.* 114, B10304. doi:10.1029/2009JB006398

COMSOL, 2020. COMSOL Multiphysics® v. 5.6. www.comsol.com. COMSOL AB, Stockholm, Sweden.

Fall, M., Nasir, O., Nguyen, T.S., 2014. A coupled hydro-mechanical model for simulation of gas migration in host sedimentary rocks for nuclear waste repositories. *Eng. Geol.* 176, 24–44. doi:10.1016/j.enggeo.2014.04.003

Flemisch, B., Darcis, M., Erbertseder, K., Faigle, B., Lauser, A., Mosthaf, K., Müthing, S., Nuske, P., Tatomir, A., Wolff, M., Helmig, R., 2011. DuMux: DUNE for multi-{phase,component,scale,physics,…} flow and transport in porous media. *Adv. Water Resour.* 34, 1102–1112. doi:10.1016/j.advwatres.2011.03.007

Garitte, B., Nguyen, T.S., Barnichon, J.D., Graupner, B.J., Lee, C., Maekawa, K., Manepally, C., Ofoegbu, G., Dasgupta, B., Fedors, R., Pan, P.Z., Feng, X.T., Rutqvist, J., Chen, F., Birkholzer, J., Wang, Q., Kolditz, O., Shao, H., 2017. Modelling the Mont Terri HE-D experiment for the Thermal–Hydraulic–Mechanical response of a bedded argillaceous formation to heating. *Environ. Earth Sci.* 76, 345. doi:10.1007/s12665-017-6662-1

Gens, A., Vaunat, J., Garitte, B., Wileveau, Y., 2007. In situ behaviour of a stiff layered clay subject to thermal loading: observations and interpretation. *Géotechnique* 57, 207–228. doi:10.1680/geot.2007.57.2.207

Ghabezloo, S., Sulem, J., 2009. Stress dependent thermal pressurization of a fluid-saturated rock. *Rock Mech. Rock Eng.* 42, 1–24. doi:10.1007/s00603-008-0165-z

Harris, C.R., Millman, K.J., van der Walt, S.J., Gommers, R., Virtanen, P., Cournapeau, D., Wieser, E., Taylor, J., Berg, S., Smith, N.J., Kern, R., Picus, M., Hoyer, S., van Kerkwijk, M.H., Brett, M., Haldane, A., del Río, J.F., Wiebe, M., Peterson, P., Gérard-

478 Marchant, P., Sheppard, K., Reddy, T., Weckesser, W., Abbasi, H., Gohlke, C.,
479 Oliphant, T.E., 2020. Array programming with NumPy. *Nature* 585, 357–362.
480 doi:10.1038/s41586-020-2649-2
481 Itasca, 2011. FLAC3d v5.0, Fast Lagrangian Analysis of Continua in 3 Dimensions, User's
482 Guide.
483 Itasca, 2016. 3DEC v5.2, Distinct-Element Modeling of Jointed and Blocky Material in 3D.
484 Itasca, 2017. FLAC3d V6.0, Fast Lagrangian Analysis of Continua in 3 Dimensions, User's
485 Guide.
486 Jung, Y., Pau, G.S.H., Finsterle, S., Pollyea, R.M., 2017. TOUGH3: A new efficient version
487 of the TOUGH suite of multiphase flow and transport simulators. *Comput. Geosci.* 108,
488 2–7. doi:10.1016/j.cageo.2016.09.009
489 Kim, J., Tchelepi, H.A., Juanes, R., 2011. Stability and convergence of sequential methods
490 for coupled flow and geomechanics: Fixed-stress and fixed-strain splits. *Comput.*
491 *Methods Appl. Mech. Eng.* 200, 1591–1606. doi:10.1016/j.cma.2010.12.022
492 Kolditz, O., Bauer, S., Bilke, L., Böttcher, N., Delfs, J.O., Fischer, T., Görke, U.J.,
493 Kalbacher, T., Kosakowski, G., McDermott, C.I., Park, C.H., Radu, F., Rink, K., Shao,
494 H., Shao, H.B., Sun, F., Sun, Y.Y., Singh, A.K., Taron, J., Walther, M., Wang, W.,
495 Watanabe, N., Wu, Y., Xie, M., Xu, W., Zehner, B., 2012. OpenGeoSys: an open-source
496 initiative for numerical simulation of thermo-hydro-mechanical/chemical (THM/C)
497 processes in porous media. *Environ. Earth Sci.* 67, 589–599. doi:10.1007/s12665-012-
498 1546-x
499 Kulik, D.A., Wagner, T., Dmytrieva, S. V., Kosakowski, G., Hingerl, F.F., Chudnenko, K.
500 V., Berner, U.R., 2012. GEM-Selektor geochemical modeling package: revised
501 algorithm and GEMS3K numerical kernel for coupled simulation codes. *Comput.*
502 *Geosci.* doi:10.1007/s10596-012-9310-6
503 Lichtner, P.C., Hammond, G.E., Lu, C., Karra, S., Bisht, G., Andre, B., Mills, R.T., Kumar,
504 J., Frederik, J.M., 2017. PLFOTRAN User Manual.
505 Lux, K.-H., Rutenberg, M., Seeska, R., Feierabend, J., Düsterloh, U., 2015. Kopplung der
506 Softwarecodes FLAC3D und TOUGH2 in Verbindung mit in situ-, laborativen und
507 numerischen Untersuchungen zum thermisch-hydraulisch-mechanisch gekoppelten
508 Verhalten von Tongestein unter Endlagerbedingungen.
509 NAGRA, 2016. Arbeitsbericht NAB 16-43: Geomechanische Unterlagen.
510 Newell, P., Martinez, M.J., Eichhubl, P., 2017. Impact of layer thickness and well orientation
511 on caprock integrity for geologic carbon storage. *J. Pet. Sci. Eng.* 155, 100–108.
512 doi:10.1016/j.petrol.2016.07.032
513 Olivella, S., Gens, A., Carrera, J., Alonso, E.E., 1996. Numerical formulation for a simulator
514 (CODE_BRIGHT) for the coupled analysis of saline media. *Eng. Comput.* 13, 87–112.
515 doi:10.1108/02644409610151575
516 Pruess, K., Oldenburg, C., Moridic, G., 2012. TOUGH2 User's Guide Version 2.1, Report
517 LBNL-43134, Lawrence Berkeley National Laboratory, Berkeley, CA, USA.
518 Rinaldi, A.P., Rutqvist, J., Cappa, F., 2014. Geomechanical effects on CO_2 leakage through
519 fault zones during large-scale underground injection. *Int. J. Greenh. Gas Control* 20,
520 117–131. doi:10.1016/j.ijggc.2013.11.001
521 Rinaldi, A.P., Rutqvist, J., Finsterle, S., Liu, H.-H., 2017. Inverse modeling of ground surface
522 uplift and pressure with iTOUGH-PEST and TOUGH-FLAC: The case of CO_2 injection
523 at In Salah, Algeria. *Comput. Geosci.* 108, 98–109. doi:10.1016/j.cageo.2016.10.009
524 Rinaldi, A.P., Vilarrasa, V., Rutqvist, J., Cappa, F., 2015. Fault reactivation during CO_2
525 sequestration: Effects of well orientation on seismicity and leakage. *Greenh. Gases Sci.*
526 *Technol.* 5, 645–656. doi:10.1002/ghg.1511
527 Rutenberg, M., Feierabend, J., Lux, K., Maßmann, J., Sentís, M.L., Graupner, B.J.,

Hansmann, J., Czaikowski, O., Wieczorek, K., Friedenberg, L., Hotzel, S., Kock, I., Rutqvist, J., Hu, M., Rinaldi, A.P., 2018. BENVASIM—A BENCHMARKING OF SIMULATORS FOR MODELING TH^{2}M PROCESSES IN THE CONTEXT OF RADIOACTIVE WASTE DISPOSAL, in: Proceedings of the TOUGH Symposium 2018. Berkeley, CA, USA.

Rutqvist, J., Wu, Y.-S., Tsang, C.-F., Bodvarsson, G., 2002. A modeling approach for analysis of coupled multiphase fluid flow, heat transfer, and deformation in fractured porous rock. *Int. J. Rock Mech. Min. Sci.* 39, 429–442. doi:10.1016/S1365-1609(02)00022-9

Rutqvist, J., 2017. An overview of TOUGH-based geomechanics models. *Comput. Geosci.* 108, 56–63. doi:10.1016/j.cageo.2016.09.007

Rutqvist, J., Rinaldi, A.P., Cappa, F.F., Jeanne, P., Mazzoldi, A., Urpi, L., Guglielmi, Y., Vilarrasa, V., 2016. Fault activation and induced seismicity in geological carbon storage – Lessons learned from recent modeling studies. *J. Rock Mech. Geotech. Eng.* 8, 789–804. doi:10.1016/j.jrmge.2016.09.001

Rutqvist, J., Zheng, L., Chen, F., Liu, H.-H., Birkholzer, J., 2014. Modeling of Coupled Thermo-Hydro-Mechanical Processes with Links to Geochemistry Associated with Bentonite-Backfilled Repository Tunnels in Clay Formations. *Rock Mech. Rock Eng.* 47, 167–186. doi:10.1007/s00603-013-0375-x

Salimzadeh, S., Paluszny, A., Zimmerman, R.W., 2018. Effect of cold CO 2 injection on fracture apertures and growth. *Int. J. Greenh. Gas Control* 74, 130–141. doi:10.1016/j.ijggc.2018.04.013

Shaw, R.P., 2015. Gas Generation and Migration in Deep Geological Radioactive Waste Repositories, Geological Society, London, Special Publications. Geological Society of London. doi:10.1144/SP415

Taron, J., Elsworth, D., 2009. Thermal–hydrologic–mechanical–chemical processes in the evolution of engineered geothermal reservoirs. *Int. J. Rock Mech. Min. Sci.* 46, 855–864. doi:10.1016/j.ijrmms.2009.01.007

Urpi, L., Rinaldi, A.P., Rutqvist, J., Wiemer, S., 2019. Fault Stability Perturbation by Thermal Pressurization and Stress Transfer Around a Deep Geological Repository in a Clay Formation. *J. Geophys. Res. Solid Earth* 124, 8506–8518. doi:10.1029/2019JB017694

van Genuchten, M.T., 1980. A Closed-form Equation for Predicting the Hydraulic Conductivity of Unsaturated Soils. *Soil Sci. Soc. Am. J.* doi:10.2136/sssaj1980.03615995004400050002x

Yapparova, A., Gabellone, T., Whitaker, F., Kulik, D.A., Matthäi, S.K., 2017. Reactive Transport Modelling of Dolomitisation Using the New CSMP++GEM Coupled Code: Governing Equations, Solution Method and Benchmarking Results. *Transp. Porous Media* 117, 385–413. doi:10.1007/s11242-017-0839-7

Zhang, C.-L., Conil, N., Armand, G., 2017. Thermal effects on clay rocks for deep disposal of high-level radioactive waste. *J. Rock Mech. Geotech. Eng.* 9, 463–478. doi:10.1016/j.jrmge.2016.08.006

SUPPLEMENTARY MATERIAL

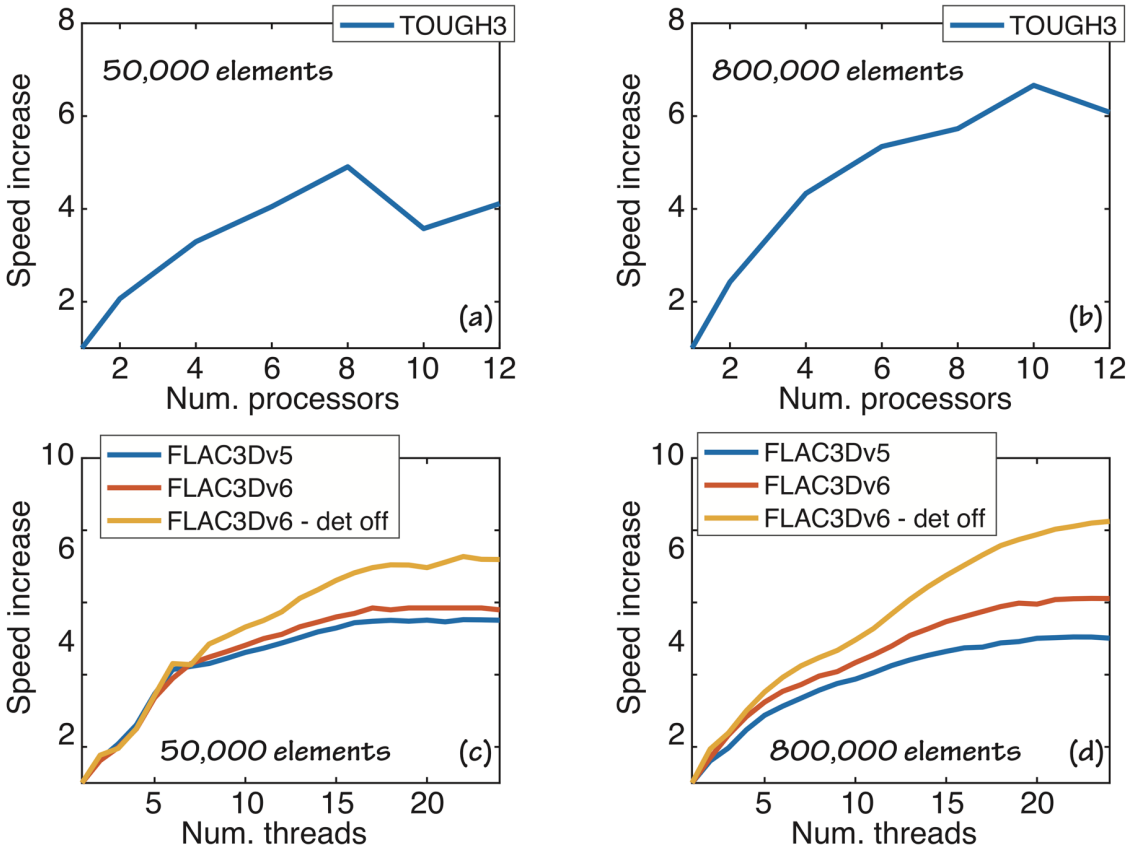

Figure S1. (a,b) Evaluation of speed increase for TOUGH3. (c,d) Evaluation of the speed increase in FLAC3D.

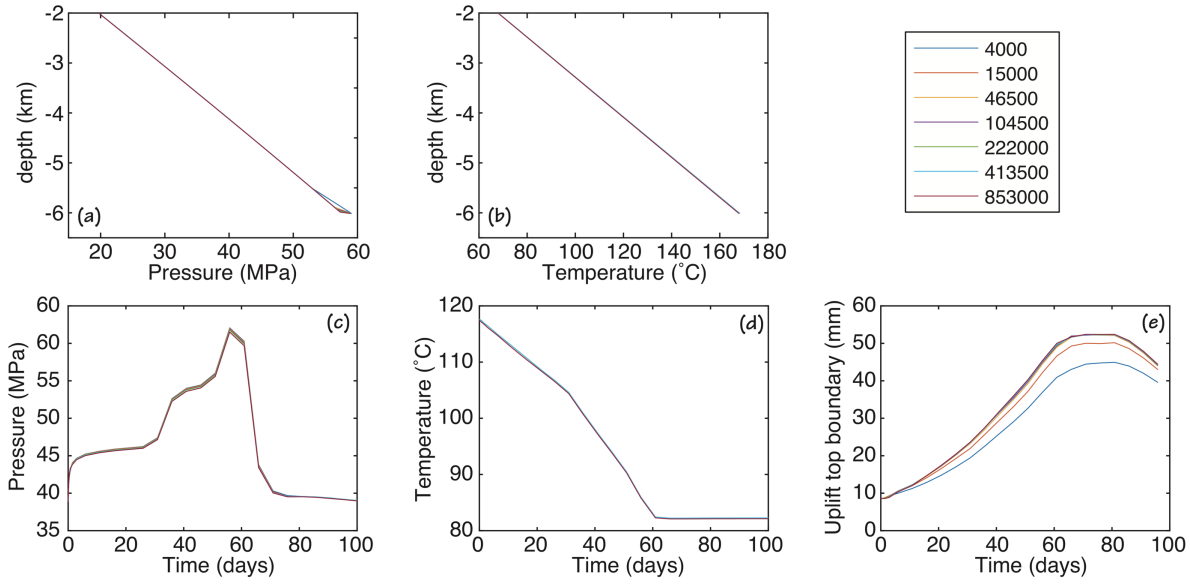

Figure S2. Simulations for different computational domain sizes: (a) Initial pressure; (b) Initial temperature; (c) Pressure evolution; (d) Temperature evolution; (e) Displacement of top boundary.